Mon. Not. R. Astron. Soc. **276,** 439–452 (1995)

Collisions of non-rotating spherical galaxies

M. Marcela Vergne★ and Juan C. Muzzio

Facultad de Ciencias Astronómicas y Geofísicas de la Universidad Nacional de La Plata and Programa de Fotometría y Estructura Galáctica del Consejo Nacional de Investigaciones Científicas y Técnicas de la República Argentina, Paseo del Bosque, 1900 La Plata, Argentina

Accepted 1995 April 3. Received 1995 March 17; in original form 1994 October 24

ABSTRACT

We have used self-consistent numerical simulations of *N*-body systems to investigate encounters between spherical non-rotating galaxies. In our simulations, the galaxies were represented by Plummer spheres ($\rho \propto r^{-5}$) with isotropic velocity distribution, and we considered collisions along hyperbolic, as well as a few parabolic, orbits. Pairs of galaxies with several different mass ratios (1:1, 1:2, 1:4 and 1:8) were included. We analysed the effects on the internal structure of the galaxies caused by collisions that did not result in mergers after one Hubble time, quantitatively estimating the changes in linear size, mass and energy, and discussing their possible correlations with the orbital parameters. Besides this, we used the results of collisions that ended up in mergers to investigate the structure of the remnants (with respect to binding energy, mass loss, linear size and flattening). We also obtained the density profiles of the remnants, which are well described by an $r^{-\gamma}$ law profile with $3 < \gamma < 3.7$.

Finally, from the analysis of collisions that ended up in mergers and of those that did not, we established a range of initial velocities and impact parameters that serves as a merging criterion.

Key words: methods: numerical – galaxies: evolution – galaxies: interactions – galaxies: structure.

1 INTRODUCTION

Over the past two decades, there has been considerable interest in the theoretical and observational consequences of collisions of galaxies, a subject recently reviewed by Barnes & Hernquist (1992) and by Muzzio (1993). Galaxies on orbits of low energy that bring them very close together usually end up merged in a single remnant after losing a relatively small amount of mass; more energetic or more distant encounters, which do not lead to mergers, can also significantly affect the structure of the galaxies involved and lead to the loss and exchange of galactic material. That exchange (dubbed *cluster swapping* by Muzzio, Martínez & Rabolli 1984, and *tidal accretion* by Muzzio 1986) is largest when the velocity difference between the galaxies is lowest (Carpintero, Muzzio & Vergne 1989), that is, for conditions close to those that lead to merging.

Unfortunately, even considering collisions of spherical non-rotating galaxies only, the parameter space is so large that much of it remains poorly explored, despite the large number of investigations performed. For example, although the ratio of the galactic masses is crucial to decide the outcome of a collision, most of the investigations performed thus far have dealt with collisions of galaxies of equal mass or of not too different mass (say, mass ratios of 1:2 or 1:3).

In the present investigation we explore galaxy collisions under conditions close to those that lead to merging. Such conditions are interesting because, on one hand, their study can result in a better knowledge of the boundary of the region of the parameter space that leads to mergers and, on the other hand, it is close to this boundary where the exchange of material between colliding galaxies is largest. Also, by limiting ourselves to this restricted region, we can explore it in more detail than we could a larger region; in particular, we want to investigate the effects of different mass ratios. Since we expect significant mass exchanges, a full *N*-body code seems better suited than one based on multipole or equivalent expansions of the potential. While the number of bodies used in the simulations must thus be low to avoid lengthy computing times, this is not a serious limitation for a preliminary exploration of the parameter space like that which we want to perform.

2 THE SIMULATIONS

2.1 Numerical simulations

We performed several *N*-body simulations of encounters of two spherical galaxies. Each galaxy was represented by a

★ E-mail address: mvergne@fcaglp.fcaglp.unlp.edu.ar.

system of identical particles, each of mass m_i, and its position defined by the vector $\boldsymbol{r}_i$; the interaction between particles i and j is defined by the potential

$$\Phi_{ij} = -G\frac{m_i m_j}{[(\boldsymbol{r}_i-\boldsymbol{r}_j)^2+\epsilon_{ij}^2]^{1/2}}, \tag{1}$$

where G is the gravitational constant and ϵ_{ij} is the softening parameter used to reduce two-body relaxation. The corresponding N-body equations of motion were integrated using a program developed, and kindly made available to us, by Dr S. J. Aarseth (Aarseth 1985). This program combines a fourth-order polynomial predictor–corrector method with the scheme developed by Ahmad & Cohen (1973), and was adapted to the HP1000 computer by Carpintero et al. (1989)

2.2 The models

We prepared seven spherical galaxies, each made up of 50, 90, 150, 225, 300, 360 and 400 particles of mass m, for our simulations. The galaxies were initially represented by non-rotating Plummer spheres with isotropic velocity distribution (Binney & Tremaine 1987, p. 223). The mass distribution within a radius r is given by

$$M(r)=\frac{\alpha r^3}{G(1+\beta r^2)^{3/2}}, \tag{2}$$

where α is a quantity proportional to the central density and β a scale factor for the distance to the centre. The total mass of the galaxy is

$$M_t=\frac{\alpha}{G\beta^{3/2}} \tag{3}$$

Since Plummer spheres have infinite radius, we truncated them at radii r_l that comprise 99 per cent of their total masses; these limiting radii are an order of magnitude larger than the half-mass radii, r_h (radii that comprise 50 per cent of the total mass). The initial parameters of the galaxies are given in Table 1: columns 1–5 list the parameters mentioned above, and columns 6 and 7 give the total internal energy (E_0) and the internal velocity dispersion (σ_0), respectively. All these parameters are expressed in our own units, which are such that $G=1$, $m=1$ and $\epsilon=1$. The scaling to real galaxies can be obtained by comparing the galaxy made up of 360 particles to galaxy M87, taking a visual absolute magnitude of $M_V=-22.3$ (Harris & Racine 1979), and the parameters α and β given by Muzzio et al. (1984). Therefore, the masses and half-mass radii of real galaxies are related to those of our models by the relations

$$M_g=M_t\mu, \qquad r_{hg}=r_h\lambda, \tag{4}$$

where $\mu=5.64\times10^{10}\,M_\odot$ and $\lambda=8.24$ kpc, and the time unit is $\tau=0.5\times10^8$ yr. Crossing times range between 4.7 and 8.6 of our time units, corresponding to galaxies with 50 and 400 particles, respectively.

We chose the softening parameter taking into account the results of White (1978), who had used galaxies made up of 250 particles. In order to have the same resolution for the different galaxy models, the softening parameter should have been reduced for the smaller galaxies. On the other hand the smaller galaxies are those that have fewer particles, thus to avoid altering the relaxation time a larger softening parameter would be needed for them. We have therefore adopted a middle-of-the-road approach, and used the same softening parameter for all the models. Some resolution is obviously lost for the smaller galaxies, but relaxation effects are kept at bay.

Before using them for our collision experiments, our model galaxies were allowed to evolve in isolation for 3.5 crossing times in order to let them reach a stable configuration. Due to the use of a softened potential and the imposition of a limiting radius, the evolved galaxies are slightly more concentrated than the original ones.

2.3 Initial conditions

Only two parameters are needed to describe the orbital motion of two galaxies: the impact parameter and the velocity at maximum separation (or at infinity). We used four mass ratios for the colliding galaxies: 1:1, 1:2, 1:4 and 1:8, with the combined mass of both galaxies always being 450 particles. The separation of the galaxies at the start of the simulation was large enough [200 units, i.e. approximately 10 times $(r_{h1}+r_{h2})$] for the initial tidal effects to be negligibly small. Hyperbolic and parabolic orbits were used for our models. We adopted pericentric distances of 0 (head-on), 10, 15, 20 and 30 units [approximately corresponding to 0, 1/2, 3/4, 1 and 3/2 of $(r_{h1}+r_{h2})$, respectively]. The orbital velocities for the hyperbolic cases were selected by choosing orbital energies that were different fractions, c, of the total internal energy of both galaxies:

$$E_{orb}=c|M_1E_1+M_2E_2|, \tag{5}$$

Table 1. Initial parameters of the galaxies.

M_t	r_h	r_l	α	β	E_o	σ_o
50	4.71	44.1	1.060	0.0766	− 120.	0.887
90	6.33	59.1	0.790	0.0726	− 284.	0.835
150	8.17	76.3	0.612	0.0255	− 506.	1.106
225	10.00	93.5	0.500	0.0170	− 787.	1.278
300	11.55	107.9	0.433	0.0128	−1473.	1.272
360	12.65	118.2	0.395	0.0106	−1932.	1.305
400	13.30	124.6	0.375	0.0096	−2581.	1.288

with $0 \leq c < 1$; E_{orb} is the orbital energy, E_i (with $i = 1, 2$) the internal energy per unit mass of the ith galaxy, and M_i its mass. The X–Y plane was chosen as the orbital plane, and the initial orbital velocity was in the x-direction. Table 2 lists the initial orbital parameters for the experiments. The first column gives the model identification ('H' indicates hyperbolic, and 'P' parabolic, orbits. The number following the letter indicates the run number). The following columns give the mass ratio (M_1/M_2), the pericentric distance (R_0 in our units, computed when taking the galaxies as point masses), the initial orbital velocity normalized with respect to the parabolic velocity at the same point (V_{rel}/V_p), the fraction c (0.0 corresponds to a parabolic orbit), and the parameters $\langle E \rangle$ and $\langle R \rangle$ that represent the normalized orbital energy and impact parameter, and which are defined below.

The evolution was followed for an interval equal to the Hubble time ($T_H = 1.5 \times 10^{10}$ yr). If the galactic pair merged during this interval and the remnant reached virialization, the run was stopped, but if the remnant was not in equilibrium, the simulation was followed until equilibrium was reached.

The analysis of the results was performed in the system of the centre of mass, which was computed in the following way. The centre of mass of each one of the two galaxies (when they had not merged), or that of the remnant (when they had merged), was computed, and the particles with positive energy with respect to this centre of mass were found; a new centre of mass was determined after excluding those particles, and the procedure was iterated until convergence was reached (after three or four iterations in most cases).

Due to the low number of particles in the small galaxy of the pair with mass ratio 1:8, the results are in some cases of low weight, and therefore only values for the other mass ratios will be provided in what follows.

3 MERGING CRITERION

We analysed a large number of experiments in order to develop a criterion for the merging of pairs of non-rotating spherical galaxies with mass ratios of 1:1, 1:2, 1:4 and 1:8. This criterion differs from those formulated previously by Aarseth & Fall (1980) and Binney & Tremaine (1987), in that they only considered galaxies of equal mass.

Each encounter of two galaxies was characterized by two dimensionless parameters, $\langle E \rangle$ and $\langle R \rangle$, which depend on the orbital properties of the galaxies and are defined as

$$\langle E \rangle = \frac{E_{orb}}{(E_1 + E_2)}, \qquad \langle R \rangle = \frac{R_0}{(r_{h1} + r_{h2})}, \tag{6}$$

where E_{orb} is the initial orbital energy, E_i (with $i = 1, 2$) is the internal energy of the ith galaxy, R_0 is the pericentric distance and r_{hi} is the half-mass radius of the ith galaxy. With these definitions, the possibility that the two galaxies were not equal is taken into account in the dimensionless parameters $\langle E \rangle$ and $\langle R \rangle$, which are listed in columns 6 and 7 of Table 2.

In this way, each initial orbit is associated with a point in the $(\langle E \rangle, \langle R \rangle)$ plane, as shown in Fig. 1. Four curves, one for each mass ratio, divide the $(\langle E \rangle, \langle R \rangle)$ space into an upper-left region, where mergers do not occur within a Hubble time, and a lower-right region, where galaxies merge within this time.

By averaging the values of the last model that did not merge with those of the first one that merges, we obtained the least-squares best fits for each mass ratio:

$$\begin{aligned}
&1{:}1 \quad \langle R \rangle = (2.33 \pm 0.04)\langle E \rangle + (1.06 \pm 0.01),\\
&1{:}2 \quad \langle R \rangle = (3.70 \pm 0.90)\langle E \rangle + (1.28 \pm 0.18),\\
&1{:}4 \quad \langle R \rangle = (7.39 \pm 0.64)\langle E \rangle + (1.51 \pm 0.08),\\
&1{:}8 \quad \langle R \rangle = (16.76 \pm 0.79)\langle E \rangle + (1.18 \pm 0.04).
\end{aligned} \tag{7}$$

We notice from Fig. 1 that when $\langle R \rangle = 0.0$, that is, when the encounter is head-on, there is a maximum energy $\langle E_{max} \rangle$, and therefore a maximum encounter speed, such that all encounters that start with $\langle E \rangle$ smaller than $\langle E_{max} \rangle$ lead to a

Table 2. Main parameters of the experiments.

RUN	M_1/M_2	R_o	V_{rel}/V_p	c	$< E >$	$< R >$
$H1$	1.0	0.0	2.20	50.0	−0.44	0.0
$H2$	1.0	0.0	1.71	25.0	−0.22	0.0
$H3$	1.0	0.0	1.18	5.0	−0.044	0.0
$H4$	1.0	10.0	1.47	15.0	−0.13	0.5
$H5$	1.0	10.0	1.18	5.0	−0.044	0.5
$H6$	1.0	15.0	1.18	5.0	−0.044	0.75
$H7$	1.0	20.0	1.04	1.0	−0.009	1.0
$P1$	1.0	0.0	1.00	0.0	+0.0	0.0
$P2$	1.0	10.0	1.00	0.0	+0.0	0.5
$P3$	1.0	20.0	1.00	0.0	+0.0	1.0
$H8$	0.5	0.0	2.05	36.0	−0.33	0.0
$H9$	0.5	10.0	1.58	17.0	−0.15	0.51
$H10$	0.5	10.0	1.46	13.0	−0.12	0.51
$H11$	0.5	20.0	1.09	2.0	−0.019	1.01
$H12$	0.5	20.0	1.05	1.0	−0.01	1.01
$H13$	0.5	30.0	1.01	0.2	−0.002	1.52
$P4$	0.5	0.0	1.00	0.0	+0.0	0.0
$P5$	0.5	10.0	1.00	0.0	+0.0	0.51
$P6$	0.5	20.0	1.00	0.0	+0.0	1.01
$H14$	0.25	0.0	1.88	19.0	−0.174	0.0

Table 2 – *continued*

RUN	M_1/M_2	R_o	V_{rel}/V_p	c	$< E >$	$< R >$
*H*15	0.25	0.0	1.45	8.0	−0.073	0.0
*H*16	0.25	10.0	1.68	13.3	−0.12	0.53
*H*17	0.25	10.0	1.57	10.6	−0.097	0.53
*H*18	0.25	10.0	1.45	8.0	−0.073	0.53
*H*19	0.25	10.0	1.17	2.7	−0.024	0.53
*H*20	0.25	20.0	1.01	0.1	−0.001	1.05
*H*21	0.25	30.0	0.66	0.05	−.001	1.58
*P*7	0.25	0.0	1.00	0.0	+0.0	0.0
*P*8	0.25	10.0	1.00	0.0	+0.0	0.53
*H*22	0.125	0.0	1.08	7.0	−0.062	0.0
*H*23	0.125	0.0	1.49	5.0	−0.045	0.0
*H*24	0.125	10.0	1.29	2.7	−0.024	0.56
*H*25	1.0	0.0	2.52	70.0	−0.61	0.0
*H*26	1.0	0.0	2.28	55.0	−0.48	0.0
*H*27	1.0	10.0	1.92	35.0	−0.31	0.5
*H*28	1.0	10.0	0.82	30.0	−0.26	0.5
*H*29	1.0	15.0	1.33	40.0	−0.34	0.75
*H*30	1.0	15.0	1.20	30.0	−0.26	0.75
*H*31	1.0	15.0	0.59	20.0	−0.17	0.75
*H*32	1.0	20.0	1.05	20.0	−0.18	1.00
*H*33	1.0	20.0	0.88	10.0	−0.09	1.00
*H*34	1.0	20.0	0.18	5.0	−0.044	1.0
*H*35	1.0	30.0	0.04	1.0	−0.009	1.5
*H*36	1.0	30.0	0.01	0.25	−0.002	1.5
*P*9	1.0	30.0	0.00	0.0	+0.0	1.5
*H*37	0.5	0.0	0.34	50.0	−0.41	0.0
*H*38	0.5	0.0	1.48	45.0	−0.41	0.0
*H*39	0.5	10.0	1.42	40.0	−0.37	0.51
*H*40	0.5	10.0	1.35	35.0	−0.32	0.51
*H*41	0.5	10.0	0.92	30.0	−0.27	0.51
*H*42	0.5	10.0	0.70	21.0	−0.19	0.51
*H*43	0.5	10.0	0.64	19.0	−0.17	0.51
*H*44	0.5	15.0	1.27	30.0	−0.28	0.76
*H*45	0.5	15.0	1.19	25.0	−0.23	0.76
*H*46	0.5	15.0	1.67	20.0	−0.18	0.76
*H*47	0.5	20.0	1.67	20.0	−0.18	1.01
*H*48	0.5	20.0	1.38	10.0	−0.092	1.01
*H*49	0.5	20.0	0.84	7.0	−0.064	1.01
*H*50	0.5	30.0	0.87	8.0	−0.073	1.51
*H*51	0.5	30.0	0.80	5.0	−0.046	1.51
*H*52	0.5	30.0	1.07	1.0	−0.014	1.51
*H*53	0.5	30.0	1.05	1.0	−0.01	1.51
*H*54	0.25	0.0	2.26	30.0	−0.27	0.00
*H*55	0.25	0.0	2.15	27.0	−0.24	0.00
*H*56	0.25	0.0	1.34	23.0	−0.21	0.0
*H*57	0.25	10.0	1.88	19.0	−0.174	0.53
*H*58	0.25	10.0	1.78	16.0	−0.15	0.53
*H*59	0.25	20.0	1.15	15.0	−0.136	1.05
*H*60	0.25	20.0	1.02	10.0	−0.091	1.05
*H*61	0.25	30.0	1.54	10.0	−0.091	1.58
*H*62	0.25	30.0	1.30	5.0	−0.046	1.58
*H*63	0.25	30.0	0.70	1.0	−0.091	1.58
*H*64	0.25	30.0	1.04	0.5	−0.006	1.58
*H*65	0.25	30.0	1.01	0.1	−0.001	1.58
*H*66	0.125	0.0	2.39	19.0	−0.174	0.0
*H*67	0.125	0.0	1.18	9.0	−0.08	0.0
*H*68	0.125	10.0	1.72	8.0	−0.071	0.56
*H*69	0.125	10.0	0.98	5.0	−0.045	0.56
*H*70	0.125	20.0	0.98	5.0	−0.045	1.11
*H*71	0.125	20.0	0.74	1.0	−0.009	1.11
*H*72	0.125	30.0	1.62	5.0	−0.045	1.67
*H*73	0.125	30.0	1.22	1.0	−0.009	1.67

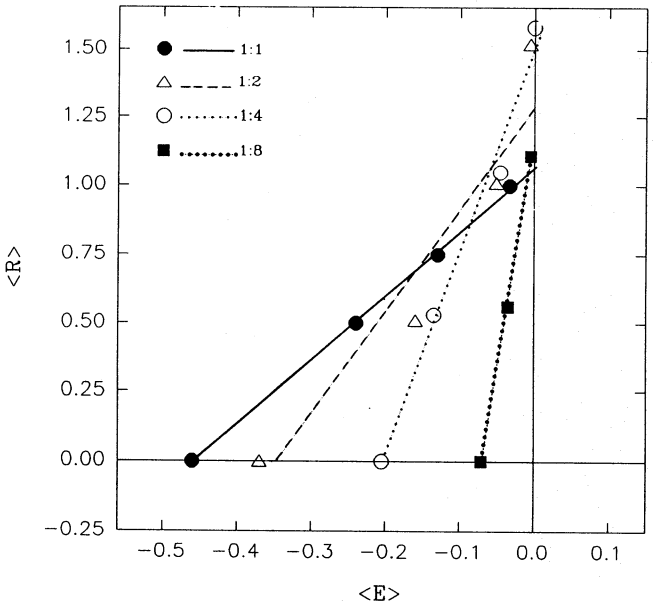

Figure 1. The $(\langle E\rangle, \langle R\rangle)$ plane. Orbits below and to the right of the limiting lines end up in mergers in a Hubble time, but the merging time increases towards the upper-left region.

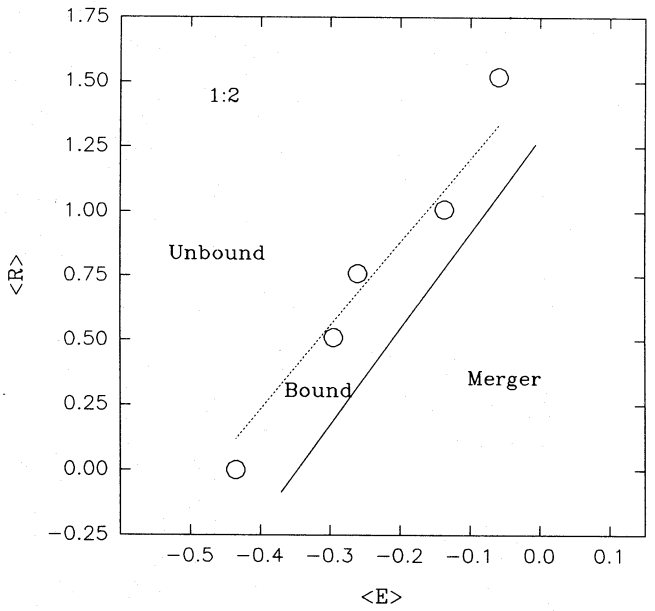

Figure 2. The $(\langle E\rangle, \langle R\rangle)$ plane, including the same curve shown in Fig. 1 (full line) for mass ratio 1:2, plus the curve (dashed line) corresponding to the case where the galaxies become bounded in a Hubble time, but take a longer time to merge. This plane is divided in three regions: unbound, bound (but not merged) and merged.

merger in one Hubble time. The value of $\langle E_{max}\rangle$ depends on the mass ratio:

1:1 $\langle E_{max}\rangle = -0.46$,

1:2 $\langle E_{max}\rangle = -0.35$,

1:4 $\langle E_{max}\rangle = -0.21$,

1:8 $\langle E_{max}\rangle = -0.07$.

For $\langle E\rangle$ values between 0.0 and $\langle E_{max}\rangle$, the collisions that end up in mergers have a limiting maximum value for $\langle R\rangle$. For our hyperbolic models, there cannot be mergers when $R_0 > 1.0(r_{h1} + r_{h2})$ for mass ratio 1:1, $R_0 > 1.25(r_{h1} + r_{h2})$ for 1:2 and $R_0 > 1.5(r_{h1} + r_{h2})$ for 1:4; the models with mass ratio 1:8 show a similar tendency, but the limiting value is uncertain due to the steep slope of the $\langle R\rangle$ versus $\langle E\rangle$ relation. For $\langle R\rangle \leq 0.75$ the limiting values of $\langle E\rangle$ are fairly different for each mass ratio, but the curves become closer for values of $\langle R\rangle$ larger than 0.75. As the mass ratio decreases, so does the dependence on the orbital momentum (or $\langle R\rangle$).

The position of the merging limits depends on the definition of the merging time (T_M), which is the interval from the initial instant (when the galaxies are at a distance D_0 from each other) to the time when the galaxies do not separate any more. Fig. 2 presents, for mass ratio 1:2, as an example, the same limit shown in Fig. 1 (full line), together with the limiting curve for the case where the galaxies become bounded in one Hubble time, but take a longer time to end up merged (dashed line). In this way, the $(\langle E\rangle, \langle R\rangle)$ plane is divided into three regions: unbound, bound-and-no-merger, and merger. It can be noticed that the full and dashed curves are roughly parallel, and not too distant from each other, which means that the curves will not change much if we adopt a different standard galaxy to estimate our time-scale; the same happens for the other mass ratios.

4 ENCOUNTERS OF GALAXIES

In the present section, we analyse the changes in the internal structure of the galaxies that did not end up merged within one Hubble time. Therefore, we only consider here the initial orbital parameters that do not satisfy the merging criterion found in Section 3; the analysis of merger remnants is left for the next section.

The results of our experiments are given in Table 3. The time chosen to evaluate the results was dubbed T_{max} (expressed in units of the Hubble time, column 2), and was defined as the time when the separation between the galaxies reached the value D_{max} (see column 3). If the pair of galaxies is unbound at T_H ($E_{orb} > 0.0$), then D_{max} is approximately equal to the initial separation, $D_0 = 200$ units; but if the pair is bound, then D_{max} is the largest separation that the galaxies reach after the first close passage. Since none of our pairs of galaxies needed more than one passage to become a bound system, the analysis of the results is limited to the first pericentral passage.

4.1 Mass loss

When one stellar system suffers an encounter with another, its velocity distribution function changes and some stars may acquire enough kinetic energy to escape from the system (*tidal stripping*). Part of the material lost by one system may be captured by the other one (*tidal accretion*).

The fractional mass change (in absolute value) of each galaxy (δM) is given in Table 3 (in the models with unequal galaxies the first line corresponds to the parameters of the small galaxy, and the second line to those of the large galaxy), and it includes the losses due to escapes from the system

Table 3. Main results of collisions.

RUN	T_{max}	D_{max}	δM	δM_e	δM_c	δE_i	$\delta\Sigma_v$	F_{zx}	F_{yx}	δr_h
*H*25	0.43	296.0	0.156	0.134	0.022	−0.515	−0.165	1.158	1.168	+0.596
			0.124	0.093	0.031	−0.459	−0.130	0.979	1.028	+0.499
*H*26	0.56	147.9	0.182	0.155	0.027	−0.497	−0.101	1.094	1.075	+0.401
			0.227	0.174	0.053	−0.538	−0.095	1.080	1.105	+0.314
*H*27	0.40	222.8	0.067	0.045	0.022	−0.163	−0.072	0.963	0.976	+0.098
			0.107	0.054	0.052	−0.156	−0.156	0.989	0.989	+0.303
*H*28	0.56	154.4	0.107	0.076	0.031	−0.280	−0.034	1.101	0.985	+0.139
			0.160	0.102	0.058	−0.410	−0.182	1.101	1.047	+0.373
*H*29	0.38	245.4	0.053	0.035	0.018	−0.136	−0.162	1.031	0.982	+0.185
			0.076	0.028	0.048	−0.288	−0.153	0.937	0.983	+0.214
*H*30	0.50	213.8	0.111	0.071	0.040	−0.280	−0.035	1.039	1.025	+0.036
			0.098	0.054	0.044	−0.330	−0.039	1.067	0.983	+0.139
*H*31	0.79	232.8	0.093	0.057	0.036	−0.215	+0.011	0.982	1.008	+0.224
			0.133	0.049	0.084	−0.304	−0.007	0.982	1.008	+0.299
*H*32	0.42	203.6	0.071	0.035	0.036	−0.145	−0.093	1.017	1.016	+0.650
			0.071	0.027	0.044	−0.193	−0.103	1.026	0.958	+0.077
*H*33	0.50	125.8	0.080	0.032	0.049	−0.226	−0.137	1.086	1.004	+0.710
			0.107	0.049	0.058	−0.297	−0.118	1.070	0.996	+0.258
*H*34	0.63	214.2	0.053	0.022	0.031	−0.130	+0.050	1.043	1.037	+0.011
			0.084	0.035	0.049	−0.106	−0.044	1.043	1.027	+0.010
*H*35	0.68	216.1	0.036	0.009	0.027	−0.100	−0.013	1.047	1.003	+0.016
			0.027	0.009	0.018	−0.069	−0.108	0.994	0.998	+0.104
*H*36	0.64	218.0	0.027	0.009	0.018	−0.064	−0.105	1.009	0.993	+0.119
			0.031	0.018	0.013	−0.060	+0.013	1.006	0.983	+0.016
*P*9	0.72	220.8	0.040	0.004	0.036	−0.086	−0.055	0.991	1.007	+0.118
			0.044	0.018	0.026	−0.061	−0.048	1.001	0.968	+0.058
*H*37	0.40	239.5	0.233	0.180	0.053	−0.510	−0.240	1.229	1.259	+0.628
			0.033	0.023	0.010	−0.313	−0.062	1.073	1.032	+0.389
*H*38	0.73	194.9	0.293	0.240	0.053	−0.567	−0.188	1.056	0.991	+0.174
			0.043	0.033	0.010	−0.331	−0.038	1.096	1.103	+0.459
*H*39	0.42	237.2	0.193	0.120	0.073	−0.527	−0.241	1.104	0.936	+0.680
			0.037	0.017	0.020	−0.223	−0.058	1.073	1.018	+0.155
*H*40	0.43	241.1	0.187	0.134	0.053	−0.530	−0.289	1.052	0.807	+1.111
			0.037	0.017	0.020	−0.195	+0.019	1.037	1.038	+0.071
*H*41	0.47	219.6	0.280	0.187	0.093	−0.580	−0.203	0.956	0.929	+0.380
			0.037	0.024	0.013	−0.163	+0.041	1.025	1.033	+0.028
*H*42	0.56	160.4	0.220	0.180	0.040	−0.399	−0.038	0.977	0.948	−0.019
			0.033	0.026	0.007	−0.225	+0.004	0.975	0.981	+0.174
*H*43	0.63	180.1	0.200	0.153	0.047	−0.370	−0.151	0.987	0.992	+0.249
			0.037	0.020	0.017	−0.219	−0.050	1.000	1.006	+0.174
*H*44	0.40	216.7	0.207	0.114	0.093	−0.489	−0.133	1.087	1.057	+0.324
			0.037	0.017	0.020	−0.149	−0.031	1.042	1.012	+0.059
*H*45	0.47	240.8	0.213	0.126	0.087	−0.380	−0.071	1.053	0.874	+0.432
			0.047	0.027	0.020	−0.149	−0.016	0.983	0.961	+0.200
*H*46	0.50	222.0	0.167	0.114	0.053	−0.159	−0.321	0.985	0.990	+0.353
			0.047	0.020	0.027	+0.025	−0.158	1.069	1.020	−0.016
*H*47	0.44	224.5	0.113	0.073	0.040	−0.273	−0.206	1.080	1.033	+0.389
			0.030	0.013	0.017	−0.119	+0.077	1.021	1.013	+0.057
*H*48	0.82	208.9	0.140	0.107	0.033	−0.262	−0.081	0.996	0.984	+0.243
			0.023	0.010	0.013	−0.112	+0.095	0.973	0.966	−0.017
*H*49	0.61	155.4	0.167	0.094	0.073	−0.321	−0.094	1.037	1.083	+0.144
			0.023	0.016	0.007	−0.100	−0.017	0.988	0.981	+0.072
*H*50	0.50	220.3	0.067	0.027	0.040	−0.151	−0.052	1.022	1.011	−0.061
			0.010	0.007	0.003	−0.029	−0.006	1.041	1.023	−0.059
*H*51	0.61	211.9	0.080	0.053	0.027	−0.181	−0.036	1.009	0.936	+0.171
			0.013	0.010	0.003	−0.057	−0.039	0.995	1.002	+0.003
*H*52	0.58	211.9	0.080	0.053	0.027	−0.181	−0.036	1.009	0.936	+0.171
			0.013	0.010	0.003	−0.057	−0.039	0.995	1.002	+0.003
*H*53	0.72	168.0	0.127	0.080	0.041	−0.159	−0.044	0.980	0.981	−0.009
			0.027	0.024	0.003	−0.070	−0.016	1.023	0.979	−0.007
*H*54	0.39	232.2	0.311	0.200	0.111	−0.550	−0.044	1.041	1.043	+0.073
			0.008	0.005	0.003	−0.161	+0.005	1.056	1.054	+0.211

Table 3 – *continued*

RUN	T_{max}	D_{max}	δM	δM_e	δM_c	δE_i	$\delta\Sigma_v$	F_{zx}	F_{yx}	δr_h
*H*55	0.42	220.5	0.367	0.223	0.144	−0.606	−0.231	1.075	1.216	+0.548
			0.006	0.003	0.003	−0.136	+0.020	1.069	1.059	+0.200
*H*56	0.50	206.1	0.367	0.234	0.133	−0.578	−0.095	0.946	0.980	−0.226
			0.003	0.003	0.000	−0.154	+0.028	0.980	1.023	+0.237
*H*57	0.36	213.0	0.256	0.156	0.100	−0.446	+0.059	1.020	0.909	−0.158
			0.003	0.000	0.003	−0.082	+0.0004	1.072	1.000	+0.110
*H*58	0.39	202.2	0.200	0.144	0.056	−0.370	−0.012	1.046	0.991	+0.097
			0.006	0.003	0.003	−0.092	+0.016	0.984	0.981	+0.061
*H*59	0.39	207.4	0.093	0.073	0.020	−0.261	−0.016	1.026	0.978	−0.066
			0.003	0.000	0.003	−0.067	+0.004	1.012	0.990	+0.072
*H*60	0.56	247.6	0.189	0.111	0.078	−0.378	+0.038	1.047	1.009	+0.034
			0.008	0.000	0.008	−0.053	+0.065	1.021	0.990	+0.016
*H*61	0.44	223.6	0.133	0.100	0.033	−0.173	+0.032	0.991	0.913	−0.125
			0.003	0.000	0.003	−0.020	+0.057	1.001	1.019	−0.038
*H*62	0.52	210.6	0.144	0.088	0.056	−0.187	+0.059	0.995	0.993	−0.035
			0.006	0.003	0.003	−0.027	+0.031	1.018	1.014	+0.003
*H*63	0.79	204.1	0.089	0.078	0.011	−0.159	−0.060	0.954	1.022	+0.160
			0.008	0.005	0.003	−0.045	+0.088	0.991	1.003	+0.011
*H*64	0.62	205.4	0.078	0.056	0.022	−0.104	+0.114	0.995	0.966	+0.159
			0.006	0.003	0.003	−0.036	+0.065	0.991	0.974	−0.047
*H*65	0.62	216.3	0.122	0.066	0.056	−0.181	+0.069	0.922	1.010	+0.076
			0.000	0.000	0.000	−0.009	+0.055	1.020	1.007	+0.020
*H*66	0.27	203.4	0.140	0.060	0.080	−0.398	−0.218	0.854	0.972	+0.330
			0.000	0.000	0.000	−0.082	−0.056	1.041	1.014	+0.056
*H*67	0.37	209.5	0.360	0.140	0.220	−0.623	−0.272	1.061	1.048	+0.240
			0.000	0.000	0.000	−0.041	+0.023	0.994	0.987	−0.025
*H*68	0.39	204.2	0.180	0.080	0.100	−0.355	−0.261	0.941	1.027	+0.273
			0.005	0.005	0.000	−0.054	+0.065	0.941	0.955	−0.069
*H*69	0.50	209.9	0.200	0.100	0.100	−0.349	−0.358	0.950	0.912	+0.170
			0.005	0.002	0.003	−0.039	−0.018	0.974	0.984	−0.003
*H*70	0.44	217.9	0.100	0.060	0.040	−0.147	−0.212	0.965	0.996	−0.055
			0.005	0.005	0.000	−0.023	+0.058	0.957	0.997	−0.099
*H*71	0.53	211.8	0.060	0.000	0.060	−0.138	−0.223	0.986	0.864	−0.107
			0.000	0.000	0.000	−0.018	+0.045	0.992	0.986	−0.021
*H*72	0.41	216.4	0.080	0.020	0.060	−0.056	−0.100	1.167	1.096	+0.004
			0.003	0.000	0.003	−0.011	+0.041	0.989	0.963	+0.049
*H*73	0.56	207.2	0.060	0.040	0.020	−0.058	−0.140	1.012	0.984	+0.069
			0.000	0.000	0.000	−0.019	+0.046	0.980	0.992	+0.022

(δM_e) and those due to captures by the other galaxy (δM_c). The maximum mass change for the whole system is about 20 per cent for encounters with mass ratios of 1:1, 1:2 and 1:4 (16 per cent truly lost and 4 per cent swapped). The loss is smaller for a mass ratio of 1:8, with a maximum value of about 4 per cent (16 per cent truly lost and 2.4 per cent swapped). The bulk of the mass loss in collisions of galaxies of different masses comes from the smaller galaxy, with the large one contributing only a small fraction to the total loss. The total mass losses from the large galaxies of the pairs are low, for example the galaxies made up of 300 and 360 particles lose about 3 per cent (1.8 per cent through escape) and 0.5 per cent (0.2 per cent through escape) of their masses, respectively.

Fig. 3 presents the fractional mass change in the system versus the orbital parameter $\langle E \rangle$ for the different mass ratios, indicating the total mass losses with full symbols and the losses by swapping with open symbols; Fig. 4 is similar, using the orbital parameter $\langle R \rangle$ as the abscissa.

The figures show good correlation between the total mass losses and the orbital parameters; besides, the largest losses correspond in every case to the most energetic and nearly head-on encounters. From simulations of head-on encounters of equal-mass galaxies, Navarro (1988) found maximum mass losses of about 22 per cent, similar to our own values.

The losses due to swapping exhibit no dependence on the orbital parameters (Figs 3 and 4). The main sources of swapped material are of course the smaller galaxies, the balance between the losses from each galaxy becoming more even as the mass ratio decreases. The minimum mass exchange corresponds to head-on encounters with equal galactic masses, which is reasonable since in those cases the relative velocities are high to avoid mergers.

Fig. 5 presents the mass-distribution of the galaxies after the encounter (for the small galaxies of the runs H_{37} and H_{55} at T_{max}), with the same distribution for the unperturbed galaxies shown for comparison; each symbol corresponds to a different fraction of bound mass (referred to as the initial

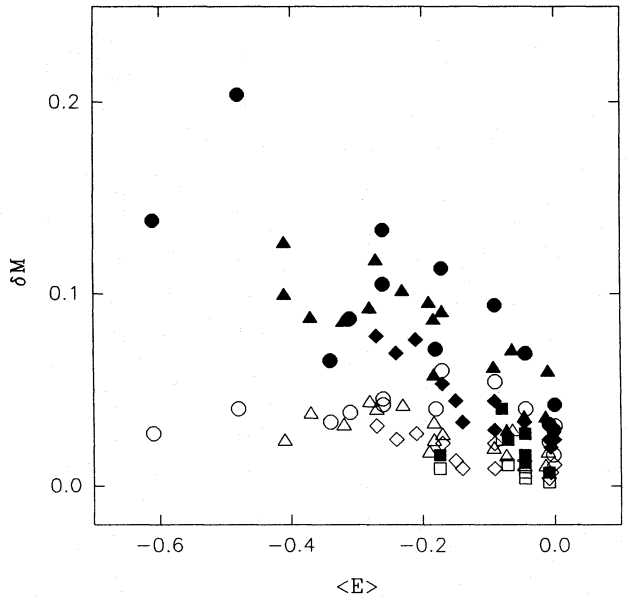

Figure 3. Fractional change in the mass of the system versus the energy parameter $\langle E \rangle$. The filled symbols correspond to the total mass loss and the open symbols to the mass loss due to swapping, for all the experiments with different mass ratios (circles for 1:1, triangles for 1:2, diamonds for 1:4 and squares for 1:8).

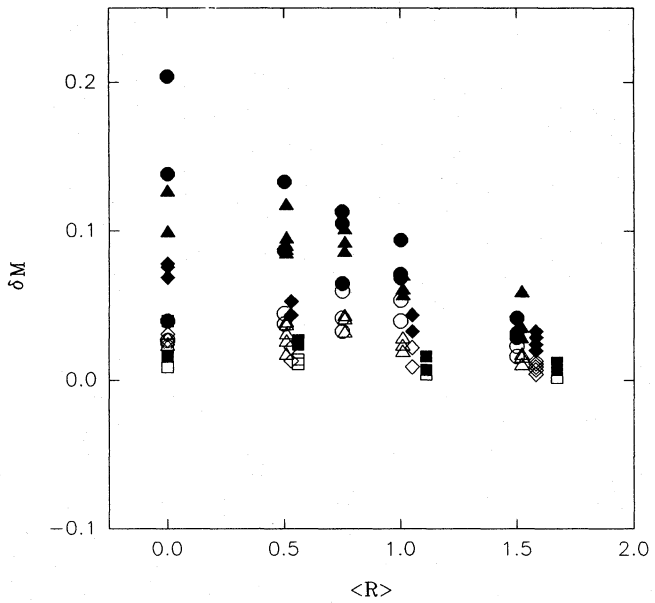

Figure 4. Fractional change in mass of the system versus the distance parameter $\langle R \rangle$. The symbols are as in Fig. 3.

mass of the galaxy, M_0). These configurations indicate that the outskirts of the galaxies lose more mass than their central parts (Fig. 5). This effect increases for energetic and interpenetrating encounters, and for lower mass ratios, especially in the least-massive companion.

4.2 Energy change

The collision of galaxies is an inelastic phenomenon, as the internal energy increases due to the loss of orbital energy

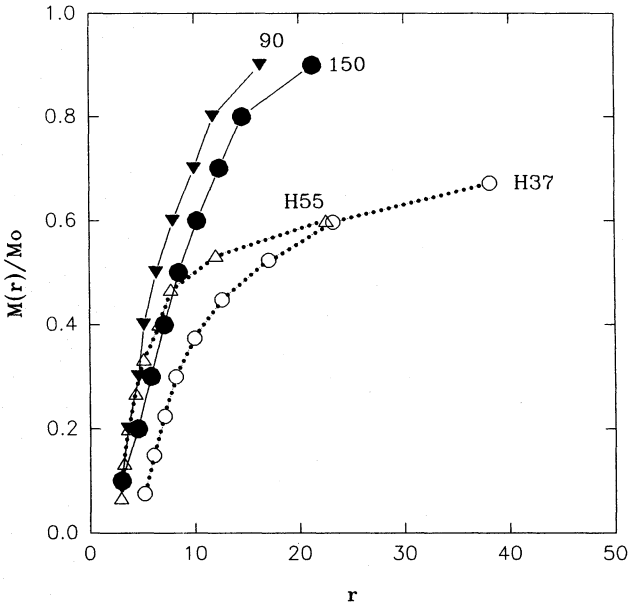

Figure 5. The final mass distribution versus the radial distance. The progenitors are indicated with filled symbols and the final configurations of the galaxies with open symbols. Each symbol corresponds to a different fraction of bound mass (referred to as the unperturbed galaxy mass, M_0).

from the colliding galaxies. The energy gained by the galaxies during the encounter is a measure of the damage they suffered.

The internal energy of a system of N particles is defined as the sum of the kinetic energies of the particles relative to their centre of mass ($\boldsymbol{r}_{CM}$) plus the potential energy of the mutual interaction, namely,

$$E_i = \sum_i \frac{1}{2} m_i (\dot{\boldsymbol{r}}_i - \dot{\boldsymbol{r}}_{CM})^2 - \frac{1}{2} \sum_i \sum_j \Phi_{ij}$$

The seventh column of Table 3 gives the fractional change in energy $\delta E_i = (E_i - E_0)/E_0$, where E_i is the energy at the final instant, (T_{max}), and E_0 is the initial energy.

Figs 6 and 7 show good correlations between the fractional change in energy and the orbital parameters ($\langle E \rangle$ and $\langle R \rangle$, respectively). In the models with different masses, the range of the change is wider for the smaller galaxies (full symbols) than for the larger ones (open symbols). Figs 3, 4, 6 and 7 show that δE_i and δM display a similar behaviour when plotted against the initial orbital parameters. Dekel, Lecar & Shaham (1980), among others, have considered a possible linear dependence between the mean mass loss ($\langle \delta M \rangle$) and the mean internal energy change ($\langle \delta E_i \rangle$). In our case, by taking

$$\delta E_i = C_M \delta M, \tag{9}$$

where C_M depends on the mass ratios, we obtained values of approximately (-2.96 ± 0.46) for a ratio of 1:1, having considered the average of the δE_i's and δM's of the pair. For models with mass ratios of 1:2, 1:4 and 1:8 the values of C_M are (-2.04 ± 0.31), (-1.61 ± 0.17) and (-1.70 ± 0.14), respectively, but when considering only the smaller galaxies. The larger galaxies lose little mass, but their internal energy

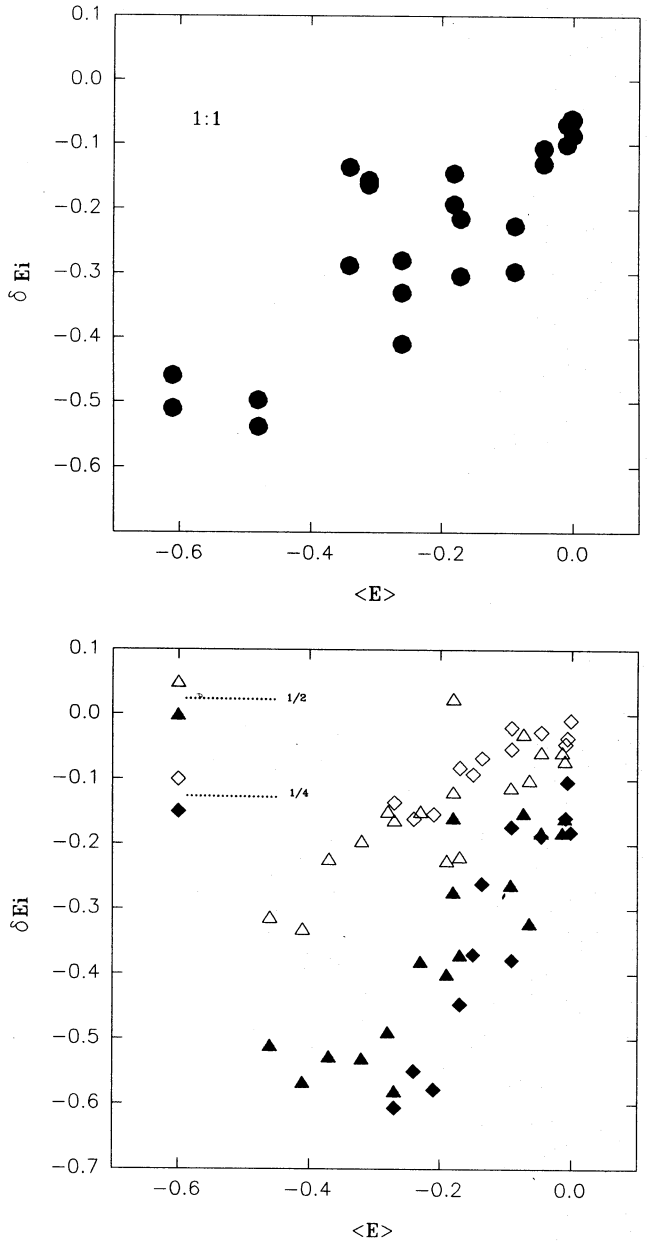

Figure 6. (a) and (b): fractional change in internal energy (δE_i) versus the energy parameter ($\langle E \rangle$), for different mass ratios (indicated in the upper-left corner of the figures). For models with unequal galaxies the filled symbols correspond to the changes in the smaller galaxy and the open symbols to those in the larger galaxy.

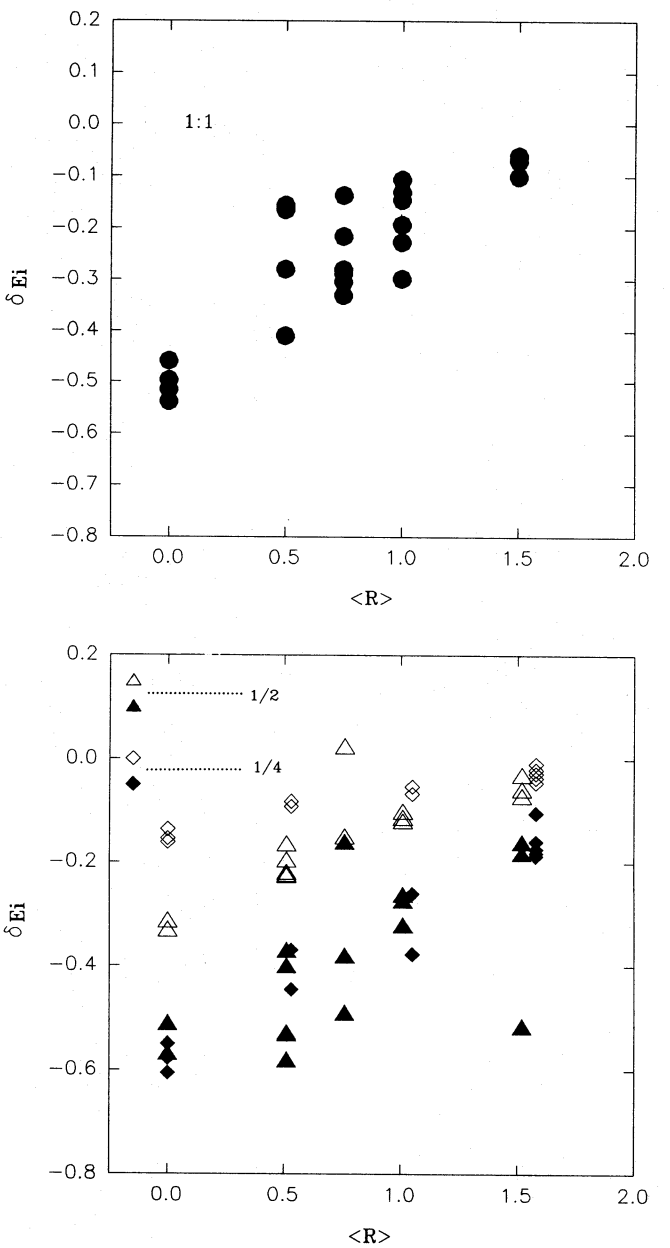

Figure 7. (a) and (b): fractional change in internal energy (δE_i) versus the distance parameter. Symbols as in Fig. 6.

suffers a larger change. Finally, the values of C_M indicate that the energy change per unit mass loss is larger for models with higher mass ratios.

4.3 Size and radial structure

The galaxies change their size as a result of the encounters and, to characterize the size of our system, and to quantify its changes, we chose the half-mass radius, r_h. In general, the results of other authors (Dekel et al. 1980; Aguilar & White 1986; Navarro 1988; Namboodiri & Kochhar 1993) show a considerable variety in the behaviour of their systems; in some cases the final system is more extended than the original one, while in others it is smaller; the outcome depends on the mass and binding energy changes, and on the mass ratio of the colliding galaxies.

The changes of our half-mass radii are given in the last column of Table 3 for each galaxy of the pair. The models with mass ratios 1:1 and 1:2 yielded, in general, galaxies that were more extended than their progenitors ($\delta r_h > 0$), as can be noticed from the corresponding mass profiles (see Fig. 8), which include the profiles of the progenitor and of the perturber galaxy, obtained by plotting the radii of the regions containing 10, 20,...,80 and 90 per cent of the mass. The central concentration of the galaxies is only slightly altered, but the outermost shells move to radii larger than the original

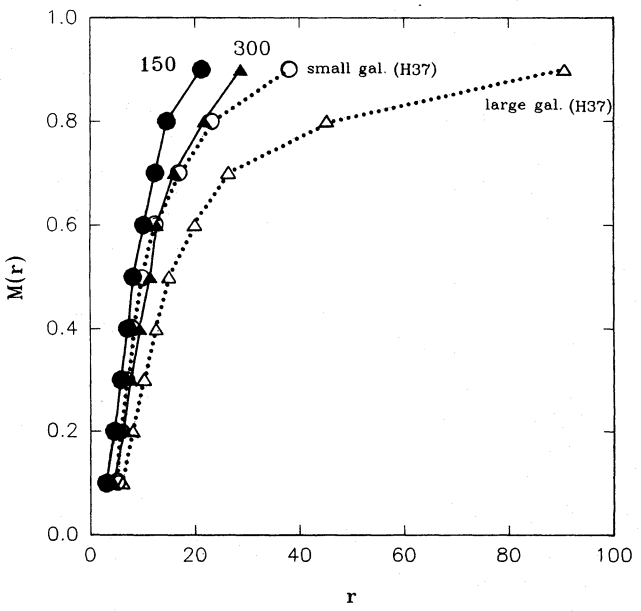

Figure 8. Final mass profiles of the galaxies evaluated at T_{max} (open symbols) and compared with the profile of the progenitor galaxy (filled symbols) for both galaxies of model H_{37}. Each symbol corresponds to given fractions of bound mass (0.1, 0.2,…, 0.9).

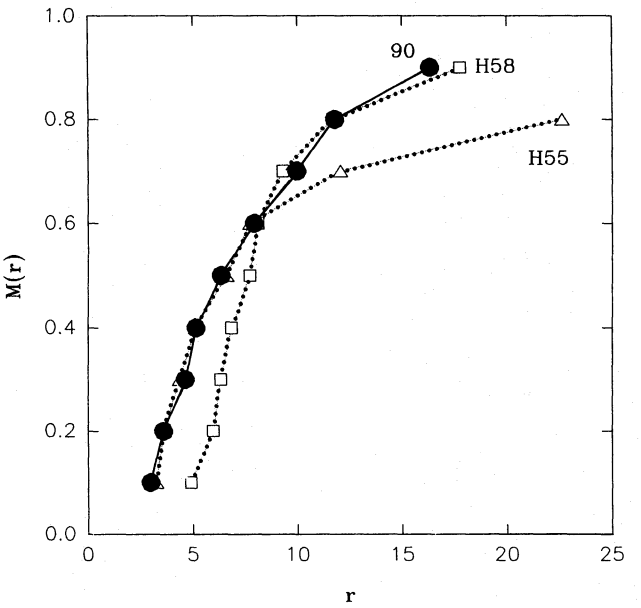

Figure 9. As in Fig. 8, but for the least massive galaxy (90 particles) of models H_{55} and H_{58}, respectively.

ones, the expansion being larger for nearly head-on encounters (strong collisions).

The smaller galaxies of the models with mass ratios 1:4 display a somewhat different behaviour, however. In some cases, the central parts of the galaxy become concentrated and the outer parts remain almost unaltered, while in others the effect is the opposite (Fig. 9). The behaviour of the larger companions is, instead, similar to that of the models with mass ratios 1:1 and 1:2.

Little can be said about the change in size of the smaller galaxy for the mass ratio of 1:8, due to the low number of particles involved. In those cases, the structure of the larger galaxy was not significantly altered by the encounters, and no differences were noticed between the results of parabolic and hyperbolic encounters.

We looked for correlations between the changes of the half-mass radii with the mass and energy changes, and with the orbital parameters, but we only found correlations with large scatter.

When the galaxies do not change their form, we would expect the change in size (δr_h) and in internal velocity dispersion ($\delta\Sigma_v$) to have opposite signs (virialized conditions). From our experiments with mass ratios of 1:1 and 1:2 we found negative $\delta\Sigma_v$ values (Table 3, column 8), in accordance with the fact that the final galaxies are less bound and have expanded ($\delta r_h > 0$), although the mass-profiles of the galaxies do not keep the homology. This departure results from the deformation of the galaxies due to the encounters, but it is not important enough to invalidate the prediction of the virial theorem under the hypothesis of homology. In the case of collisions occurring where the mass ratio is 1:4, there is instead a significant change in the mass profiles of the galaxies involved and, accordingly, the signs of δr_h and $\delta\Sigma_v$ cannot be easily predicted.

4.4 Flattening and rotation

The degrees of flattening F_{zx} and F_{yx} were computed using the formula

$$F_{ix} = \frac{N(N+1)}{K_i},$$

with $i = y, z$, N being the number of bound particles of the galaxy, and K_i the sum of the ranks of the N x-distances amongst the N y- or z-distances. This method of finding flattenings was used by White (1978), and it has the advantage that it weights each particle equally. These quantities are given in columns 9 and 10 of Table 3. In general, the galaxies tend to conserve the sphericity (F_{zx} and F_{yx} nearly equal to 1.0) or they are slightly flattened towards the orbital plane ($F_{zx} > 1$). Head-on encounters result, instead, in prolate galaxies. The least-massive members show significant fluctuations in the values of the F_{ix} factors, due to the low number of particles involved.

The rotation of the galaxies is measured by the spin parameter (λ), defined as

$$\lambda = \frac{E^{1/2}L}{GM^{5/2}},$$

where L is the modulus of the angular momentum, E is the absolute value of the total energy and M is the bound mass of the galaxy. The galaxy models initially have no rotation, and they do not acquire any significant spin from the encounters. Our spin parameters, λ, are all smaller than 0.083 and, therefore, they are lower than the values given by Farouki, Shapiro & Duncan (1983) for elliptical galaxies.

Table 4. Structural parameters of the merger remnants.

RUN	T_M	T_S	T_{Lim}	M	r_h	$\epsilon(\%)$	λ	F_{zx}	F_{yx}	E_t	Σ_v
*H*1	0.64	1.82	1.82	378	19.1	16.2	0.010	1.096	1.060	−1499.7	1.320
*H*2	0.47	1.00	1.00	400	15.8	11.0	0.010	1.058	0.980	−1904.7	1.499
*H*3	0.38	1.13	1.13	414	14.1	8.0	0.008	0.966	0.993	−2246.2	1.574
*H*4	0.67	1.67	1.67	412	18.8	8.4	0.096	0.978	0.908	−2010.0	1.438
*H*5	0.42	1.00	1.00	427	16.8	5.1	0.107	1.004	1.041	−2168.9	1.415
*H*6	0.50	1.67	1.67	434	17.8	3.8	0.132	1.074	0.960	−2160.2	1.366
*H*7	0.76	1.56	1.56	429	17.3	4.7	0.148	1.060	1.014	−2225.4	1.335
*P*1	0.32	1.36	1.36	426	15.3	5.3	0.009	1.041	1.049	−2278.4	1.477
*P*2	0.56	1.00	1.60	436	18.7	3.1	0.107	1.058	0.929	−2236.4	1.468
*P*3	0.72	1.32	1.32	429	16.7	4.7	0.145	1.012	1.017	−2247.9	1.382
*H*8	0.36	1.86	1.86	393	17.9	12.9	0.025	1.157	1.139	−1770.5	1.468
*H*9	0.95	1.53	2.05	419	20.3	6.9	0.090	1.119	1.073	−1941.2	1.484
*H*10	0.71	1.48	1.48	423	18.9	6.2	0.091	1.039	1.020	−2019.0	1.418
*H*11	0.71	1.05	1.05	425	16.5	5.6	0.128	1.045	0.980	−2207.6	1.400
*H*12	0.60	1.00	1.00	428	15.6	4.9	0.135	1.062	0.985	−2232.8	1.492
*H*13	0.48	1.00	1.00	432	18.7	4.0	0.135	1.080	0.921	−2243.7	1.422
*P*4	0.61	1.00	1.35	426	15.7	5.3	0.009	1.025	1.013	−2179.0	1.528
*P*5	0.40	1.00	1.12	428	15.3	4.9	0.092	1.011	0.961	−2249.8	1.468
*P*6	0.64	1.00	1.20	432	17.1	4.0	0.136	1.021	0.931	−2257.6	1.468
*H*14	1.00	1.45	1.45	424	15.9	5.8	0.010	1.039	1.011	−2188.9	1.346
*H*15	0.27	1.00	1.08	431	14.8	4.2	0.008	1.054	1.026	−2359.3	1.520
*H*16	0.67	1.29	1.29	426	15.4	5.3	0.061	1.079	1.017	−2270.3	1.442
*H*17	0.68	1.44	1.44	425	16.6	5.6	0.060	1.073	1.012	−2299.2	1.387
*H*18	0.77	1.00	1.00	430	16.5	4.3	0.070	1.057	0.975	−2331.0	1.376
*H*19	0.57	1.00	1.00	433	15.9	3.8	0.067	1.022	0.973	−2449.9	1.424
*H*20	0.76	1.14	1.14	434	14.6	3.6	0.094	1.005	0.953	−2494.3	1.423
*H*21	0.93	1.24	1.24	434	14.3	3.6	0.101	1.015	1.003	−2477.5	1.524
*P*7	0.31	1.34	1.34	437	16.2	2.9	0.010	1.032	0.985	−2472.0	1.454
*P*8	0.45	1.28	1.28	437	15.4	2.9	0.074	1.028	0.969	−2468.6	1.494
*H*22	0.58	1.00	1.00	438	15.6	2.7	0.007	1.013	0.994	−2590.8	1.432
*H*23	0.50	1.00	1.00	437	15.3	2.9	0.008	0.986	0.992	−2632.2	1.476
*H*24	0.76	1.00	1.07	441	13.7	2.0	0.037	1.048	1.027	−2681.7	1.411

5 MERGERS

The results from our collision models for galaxies that become merged are very similar to those obtained before by other authors (White 1978; Villumsen 1982, 1983; Navarro 1989), so that they will be only briefly discussed in the present section.

Several interesting properties are apparent from our results, which are given in Table 4. First, some mass escapes from the system during the merging process: up to about 16 per cent of the total mass for mass ratio 1:1, 13 per cent for 1:2, 5.3 per cent for 1:4 and 3 per cent for 1:8; these values correspond to experiments involving our most energetic hyperbolic encounters. The parabolic encounters lead to smaller mass losses than the mildly hyperbolic ones analysed here (about 5.3 per cent for mass ratios of 1:1 and 1:2, and 2.9 per cent for 1:4); the situation may be different for hyperbolic encounters at higher velocities. In Fig. 10 we plotted the fractional mass loss of each system versus the orbital parameter $\langle E\rangle$, as well as the least-squares linear fit, including the results from all four mass ratios

$$\epsilon(\langle E\rangle)=(-26.5\pm2.6)\langle E\rangle+(3.59\pm0.30).$$

Our experiments show that the models with mass ratios of 1:1 and 1:2 tend to yield similar numbers of escapees for the

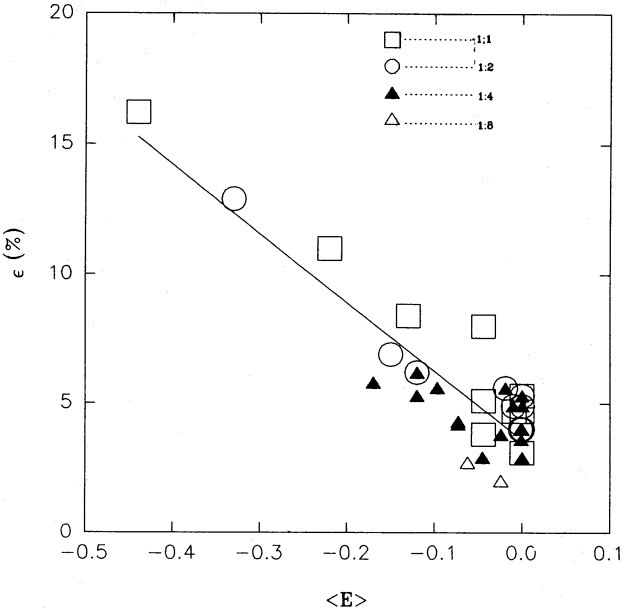

Figure 10. Mass loss versus the energy parameter ($\langle E\rangle$) for different mass ratios. The full line corresponds to a least-squares linear fit.

same orbital energy, while on the other hand, the models with mass ratios of 1:4 and 1:8 tend to lose less mass than the others. The mass loss [$\epsilon(\%)$] is listed in the seventh column of Table 4.

Another interesting feature of the merger remnants is that the systems are less bound when the number of escapees increases and, therefore, for larger mass ratios (see Fig. 11).

The rotation of the remnants is measured by the same spin parameter, λ (eighth column of Table 4), defined above. We notice from Fig. 12 (λ versus $\langle R \rangle$) that encounters that result from orbits of large angular momentum produce remnants which rotate as rapidly as $\lambda = 0.16$ (i.e., a value similar to those of elliptical galaxies), and it tends to decrease for lower mass ratios.

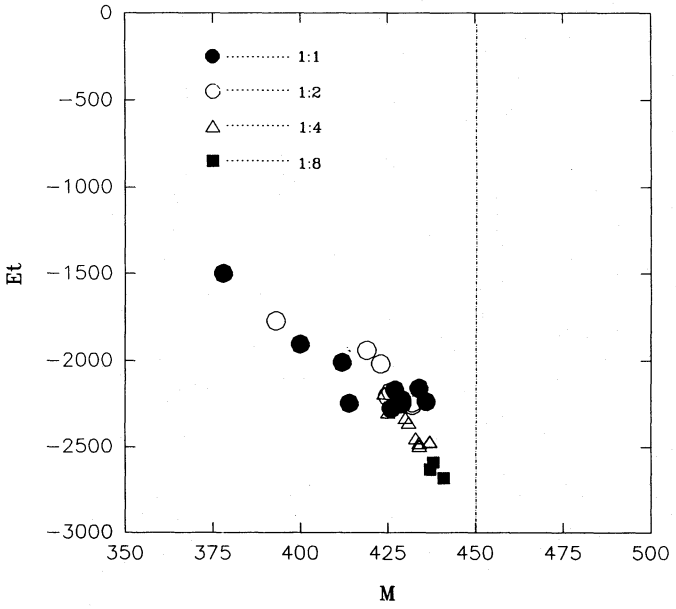

Figure 11. Final energy (E_t) versus mass of the remnant, for all the experiments.

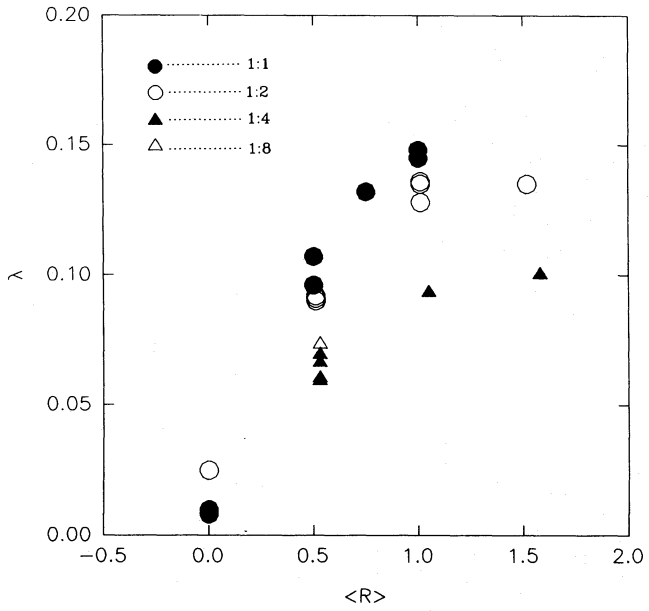

Figure 12. Rotation parameter (λ) versus distance parameter.

The remnants show a trend from 'prolate' to 'oblate' configurations as the impact parameter increases. The degree of flattening is given by the F_{zx} and F_{yx} factors defined above. Thus, head-on encounters such as those of models H_1, H_8 and H_{16} yield remnants either elongated in the initial orbital direction (x-axis), or prolate. Finally, the remnants of models with mass ratios of 1:2 and 1:4 are flatter than those of models with a mass ratio of 1:1. The parabolic encounters result in remnants similar to those of the hyperbolic models.

We use three different characteristic times for our models, given in the second, third and fourth columns of Table 4 (in units of the Hubble time). The first is the merging time T_M, defined in Section 3. The second is the virialization time T_S, the time required for the remnant to virialize (i.e., to reach $Q = T/U \simeq 0.5$). Finally, the limit time T_{Lim} is the time when the simulation was stopped and the final parameters were evaluated.

We notice that the T_M values are similar for mass ratios of 1:1 and 1:2, and that they tend to increase with increasing impact parameter. However, the merging times for mass ratios 1:4 and 1:8 are longer than those for larger mass ratios (1:1, 1:2). The reason is that T_M depends strongly on how the merging process takes place. A good example is offered by model H_{24}, that has a T_M value similar to those of models H_4 and H_{10}, although the last two are more energetic than the first one.

Models that involve equal galactic masses result in virialization times longer than one Hubble time (T_H), but this does not happen when the masses are different. In the latter case the structural parameters of the remnant are similar to those of its larger progenitor.

Fig. 13 shows the density profile for a merger remnant. The particles were binned in 10 spherical shells of equal

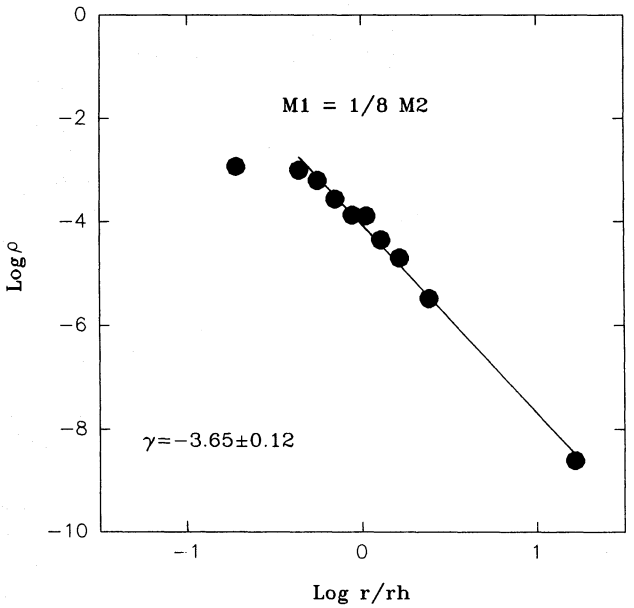

Figure 13. Density profile corresponding to the final configuration of a remnant (it corresponds to mass ratio 1:8). The abscissa is the logarithm of the radius in units of the half-mass radius, and the ordinate is the logarithm of the spatial density. The profile is well fitted by the power-law ($\rho \propto r^{\gamma}$).

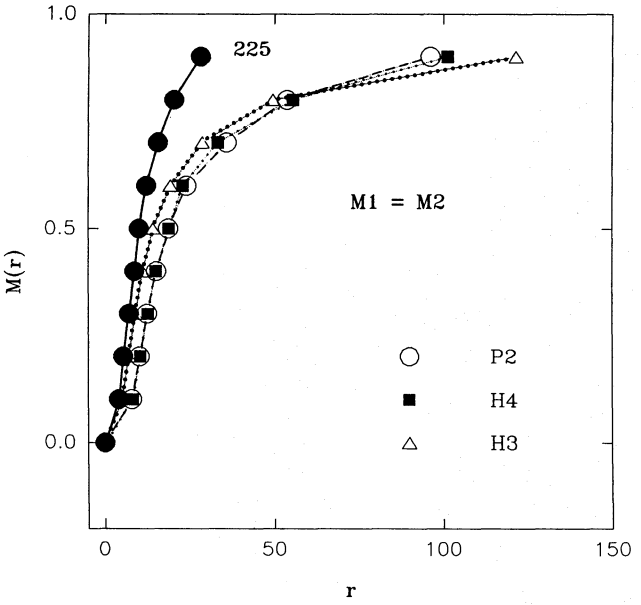

Figure 14. Mass profiles of the progenitor galaxy and of the remnants of the experiments indicated in the lower-right corner of the figure. Each symbol corresponds to a different fraction of the total mass (0.0, 0.1,…, 0.9).

volume. The radius of each shell was computed as the average of the outer and inner radii, and it was normalized to the half-mass radius (r_h). The form of the final profiles is about the same for all remnants, regardless of the initial orbital parameters and of the galactic mass ratios. They can be approximated by a power law ($\rho \propto r^{\gamma}$), with exponent between -3 and -3.7, except in the central region where the correlation is poor due to the softening. These values are characteristic of violent relaxation processes (Aarseth & Binney 1978).

The radial structure and size changes can be seen in Fig. 14, where the mass distribution of the remnants is compared with that of the progenitor galaxies. In every case the outer shells of the remnants are more extended than those of their progenitors, especially for head-on encounters with $M_1/M_2 = 1{:}1$ and 1:2.

6 CONCLUSIONS

We performed a large number of simulations for collisions of stellar systems, and obtained a good coverage of the parameter space (orbital parameters, mass ratios). Our results provide quantitative estimates of the changes undergone by the galaxies due to the collisions, and of the structural characteristics of the remnants of the mergers. In the case of encounters that did not result in mergers the main conclusions can be summarized as follows.

(i) The maximum mass loss is about 20 per cent for encounters with mass ratios of 1:1, 1:2 and 1:4 (16 per cent corresponds to true loss, and 4 per cent is swapped between the galaxies); for the mass ratio of 1:8 the maximum loss is about 4 per cent (1.6 per cent truly lost and 2.4 per cent swapped). The mass loss correlates with the orbital parameters of the collision. The mass profiles show that the galaxies lose mass mainly from their outer envelopes.

(ii) After the encounters the galaxies are less bound than before.

(iii) After head-on encounters the galaxies tend to be 'prolate', while after non-head-on encounters the galaxies either conserve approximately their spherical forms or become slightly flattened towards the orbital plane.

(iv) The final galaxies have more extended envelopes than their progenitors. Only the least massive galaxies of the models with a mass ratio of 1:4 have a different behaviour. In general, the changes in the mass profiles do not follow a homology.

From the cases where the galaxies ended up merged, we conclude the following.

(i) Our maximum mass loss from encounters on hyperbolic orbits is about 16 per cent for a mass ratio of 1:1, about 13 per cent for 1:2, about 5.3 per cent for 1:4 and about 3 per cent for 1:8. These values correspond to our most energetic encounters. On the other hand, the parabolic encounters lose less mass than the hyperbolic encounters (about 5.3 per cent for 1:1 and 1:2, and 2.9 per cent for 1:4). Note, however, that our most energetic encounters are relatively mild, and the situation may be different for higher velocities. The lost mass correlates strongly with the orbital energy of the collision.

(ii) The encounters that result from large angular momentum orbits produce remnants that rotate as rapidly as $\lambda = 0.16$. The dimensionless spin parameter decreases with decreasing mass ratio.

(iii) Remnants resulting from head-on encounters are prolate. When the pericentric distance increases, the remnants flatten to the orbital plane (oblate). The flattening of the system increases with the mass ratio.

(iv) The merging times are very long, particularly for models with small mass ratios, and they depend on how the merging process takes place.

(v) The profiles of the remnants of collisions between Plummer models ($\rho \propto r^{-5}$) are well described by an $r^{-\delta}$ power-law profile with $3 < \delta < 3.7$.

ACKNOWLEDGMENTS

We especially thank Sverre J. Aarseth for kindly making his *N*-body code available to us. We also thank S. D. Abal de Rocha, M. C. Fanjul de Correbo, R. E. Martínez and H. R. Viturro for technical assistance. This work was supported with grants from the Consejo Nacional de Investigaciones Científicas y Técnicas de la República Argentina (CONICET) and from the Fundación Antorchas.

REFERENCES

Aarseth S. J., 1985, in Brackbill J. W., Cohen B. J., eds, Multiple Time Scales. New York Academic Press, NY, p. 377
Aarseth S. J., Binney J. J., 1978, MNRAS, 185, 227
Aarseth S. J., Fall M., 1980, ApJ, 236, 4
Aguilar L. A., White S. D. M., 1986, ApJ, 307, 97
Ahmad A., Cohen L., 1973, J. Comput. Phys., 12, 389
Barnes J. E., Hernquist L., 1992, ARA&A, 30, 705
Binney J. J., Tremaine S., 1987, Galactic Dynamics. Princeton Univ. Press, Princeton
Carpintero D. D., Muzzio J. C., Vergne M. M., 1989, Celest. Mech., 45, 1

Dekel A., Lecar M., Shaham J., 1980, ApJ, 241, 946
Farouki R. T., Shapiro S. L., Duncan M. J., 1983, ApJ, 265, 597
Harris W. E., Racine R., 1979, ARA&A, 17, 241
Muzzio J. C., 1986, ApJ, 301, 23
Muzzio J. C., 1993, in Gurzadyan V. G., Pfenniger D., eds, Ergodic Concepts in Stellar Dynamics. Springer-Verlag, Heidelberg, p. 243
Muzzio J. C., Martínez R. E., Rabolli M., 1984, ApJ, 285, 7
Namboodiri P. M. S., Kochhar R. K., 1993, MNRAS, 261, 855
Navarro J. F., 1988, PhD Thesis, Córdoba University
Navarro J. F., 1989, MNRAS, 239, 257
Villumsen J. V., 1982, MNRAS, 199, 493
Villumsen J. V., 1983, MNRAS, 204, 219
White S. D. M., 1978, MNRAS, 184, 185